STRUCTURAL AND MAGNETIC PROPERTIES OF NANOPARTICLE SEMICONDUCTORS $La_{1-x}Sr_xMnO_3$

by

Zainab M. H. El-QAHTANI[a], Alaa M. ADAM[b,c*], Ahmed ELSHAFAIE[b], Eslam M.M. IBRAHIM[b], Ahmet Mohamed AHMED[b], Hanadi M. ABDELSALAM[d], Ibtisam DAQQA[d], and Khalda T. OSMAN[e]

[a] Department of Physics, College of Science,
Princess Nourah bint Abdulrahman University, Riyadh, Saudi Arabia
[b] Physics Department, Faculty of Science, Sohag University, Sohag, Egypt
[c] Faculty of Engineering, King Salman International University, South Sinai, Egypt
[d] College of Sciences and Human Studies,
Prince Mohammad Bin Fahd University, Al-Khobar, Saudi Arabia
[e] Physics Department, College of Science, Qassim University, Buraidah, Saudi Arabia

Original scientific paper
https://doi.org/10.2298/TSCI2501383E

With a view to investigate the magneto-structural properties and influence of annealing on magnetoresistance of strontium-doped lanthanum manganite, samples of $La_{1-x}Sr_xMnO_3$ were prepared and their magneto-transport properties have been investigated in this article. Magnetoresistance is enhanced from 6% to about 94% at room temperature due to annealing. Resistivity and Seebeck coefficient were investigated over the temperature range $83 \leq T \leq 313$ K. The quasi-static magnetization was investigated in the temperature range of 5-400 K under effect of a magnetic field of 100 Oe in both moods of field cooling presence besides the zero field cooling. The measurements of magnetization showed Curie transition from ferromagnetic behavior to paramagnetic one. The Curie transition values increased with increasing the strontium content suggesting that the transfer integral between two Mn sites would be enhanced due to the substitution of smaller La ions (117.2 pm) by greater Sr ions (132 pm). Various parameters were calculated from the application of variable range hopping and single polaron hopping models. Both models were utilized to investigate the effect of Sr on the conduction behavior. The behavior of thermopower with temperature was demonstrated on the basis scatterings of phonon-and magnon-.

Key words: *magnetoresistance, Curie transition, ferromagnetic region, polaron hopping, magnon-scattering*

Introduction

Rare-earth $La_{1-x}A_xMnO_3$ manganites are of high interest because of their unique magnetic characteristics. As reported, $La_{1-x}A_xMnO_3$ and based alloys show high interest in applications such as in magnetic sensors, ferroelectric memories and recording devices [1-8]. The paramagnetic/semiconductor to ferromagnetic/metal transition has been demonstrated during the double exchange between Mnions [5] besides the creation of polarons at a transition temperature [6-8]. Many attempts have been conducted to describe the conduction mechanism

* Corresponding author, e-mail: a.adam@science.sohag.edu.eg

above a transition temperature of these compounds. Some studies reported that Mott variable range hopping (VRH) model is well applied above T_{ms} but over a limited temperature range. However, intensive analyses on the conductivity and thermoelectric power data favor the small polaron hopping (SPH) due to lattice polaron formation [9-12]. Therefore, it is difficult to distinguish whether the VRH or SPH model can represent the characteristics of a semiconductor behavior. In the concerned work, we introduce a complete investigation of the electrical conduction in order to determine the models that describe the conduction mechanisms over different temperature regions. However, most of the previous studies do not take into account the location of transition temperature neither in the degenerate nor in the non-degenerate state of semiconductor which is an interesting and relevant problem to address. To be much closer to the side of the application we, experimentally, measured the magnetoresistance of the concerned samples and identified the best value at room temperature, next to that, heat treatment was carried out for enhancing magnetoresistance at room temperature. In terms of comparison, MR measurements showed relatively high values which strongly suggest applications in the field of hard disc devices and sensors manufacturing.

Experimental

$La_{1-x}Sr_xMnO_3$ (x = 0.1, 0.15, and 0.2) were first synthesized via a standard solid-state method. At the beginning, La_2O_3 (heated at 873 K for dehydration), Sr_2CO_3 and $MnCO_3$, all with purity grade 99.99%, compounds were gathered together according to the required stoichiometric amounts. The mixtures of these precursors were grounded (for 30 minutes) and compacted under a pressure of 5 tonne per cm^2 followed by calcination at 1173 K for 12 hours. Secondly, the samples were reground using ball milling for 50 hours to obtain fine powders. The milled powders were finally pressed into pellets under a pressure of 7 tonne per cm^2 and thermally treated at 1373 K for 18 hours [13]. The XRD was used to identify the induced phases and internal structure of the compositions at hand. The morphology was characterized using the SEM. The resistivity *vs*. temperature measurements were carried out using a homemade cryostat throughout the four-probe method discussed in detail in a previous work [14]. Magnetic features were characterized with the aid of a vibrating sample magnetometer from LDJ 9600 model.

Results and discussion

Structure and morphology

The morphological properties of as prepared $La_{1-x}Sr_xMnO_3$ samples (x = 0.1, 0.15, and 0.2) is shown in fig. 1. A uniform grains distribution is obvious in all samples. Clearly, porosity decreases, and the samples become denser as the Strontium content increases. It is noted that the average size of grains decreases as the Sr content increases. Noteworthy, the grain size (GS) and grain morphology have significant effect on the transport and magneto-transport properties of the manganites [15, 16]. The XRD patterns are given in fig. 1 for $La_{1-x}Sr_xMnO_3$ (x = 0.1, 0.15, and 0.2) samples. The data revealed rhombohedral perovskite structure with space group $R\bar{3}c$ which is well known for $La_{1-x}Sr_xMnO_3$ (LSMO) compounds [17-19]. No indication of the existence of impurity phases could be detected even at higher Sr concentration levels. The normalized intensity of the most intense peak (observed at $2\theta \approx 32.22°$) is improved significantly with x increase indicating a crystallization favorability in this direction. Changing the Sr content in the composition is associated with favorability of crystalline orientations in certain directions. For instance, the peak at $2\theta \approx 22.5°$ appears for the $x \geq 0.15$ sample although it is not observed for the samples with the lowest Sr content (x = 0.1). A significant effect of Sr content on the

width of the induced peaks can be observed. To be more specific, the induced peaks become broader as the Sr content increases indicating a notable reduction of the crystallite size (CS). It is clear from tab. 1 that for the same sample the GS is much higher than the CS because the former composes of many crystallites besides stresses and/or structural defects [20].

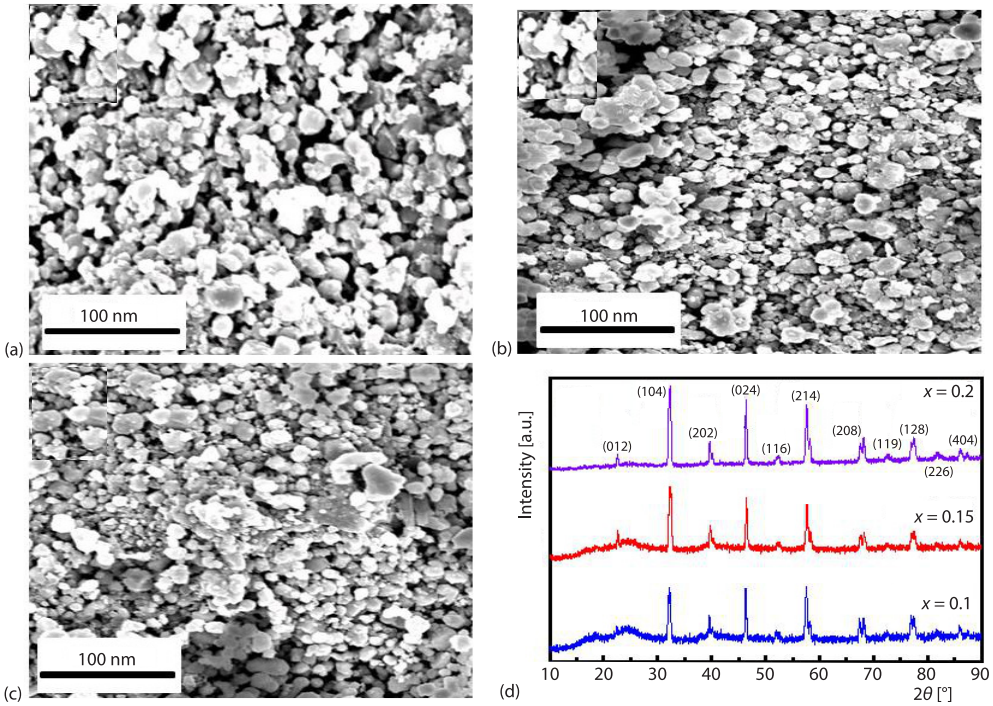

Figure 1. The SEM images of $La_{1-x}Sr_xMnO_3$; (a) $x = 0.1$, (b) 0.15, (c) 0.2, and (d) XRD

Table 1. The CS and GS as determined from the XRD and SEM results, respectively, T_{ms}, T_{MR}, and T_c $La_{1-x}Sr_xMnO_3$ samples

x	0.1	0.15	0.2
CS_{XRD} [nm]	48	58	68
GS_{SEM} [nm]	132	136	152
T_{ms} [K]	113	113	123
T_{MR} [K]	140	151	123
T_c [K] Zero field cooled	113	123	170

Electrical properties

Temperature dependency of resistivity with/without external applied DC magnetic field ($H = 0.5T$) was studied within the temperature range ($83 \leq T \leq 313$ K) as depicted in fig. 2. For easier comparison the Lnρ-T plot of $H = 0.5T$ magnetic field for a distinct sample is presented together with that of zero magnetic field in one figure, fig. 2. Similarly, lnρ-T variation measured at $0.5T$ for all compositions show the transition from metallic to semiconducting behavior. It can be observed from fig. 3 that each MR-T variation shows a maximum at a certain temperature, T_{MR}. The T_{MR} values were found to be comparable with those of T_{ms}, see tab. 1 and

fig. 2(d). Noteworthy the highest MR value at room temperature was determined to be 6.6% and recorded for the $x = 0.15$ sample. As a rebuttal to this point, it might be convincingly argued the effect of annealing on this sample in the following section.

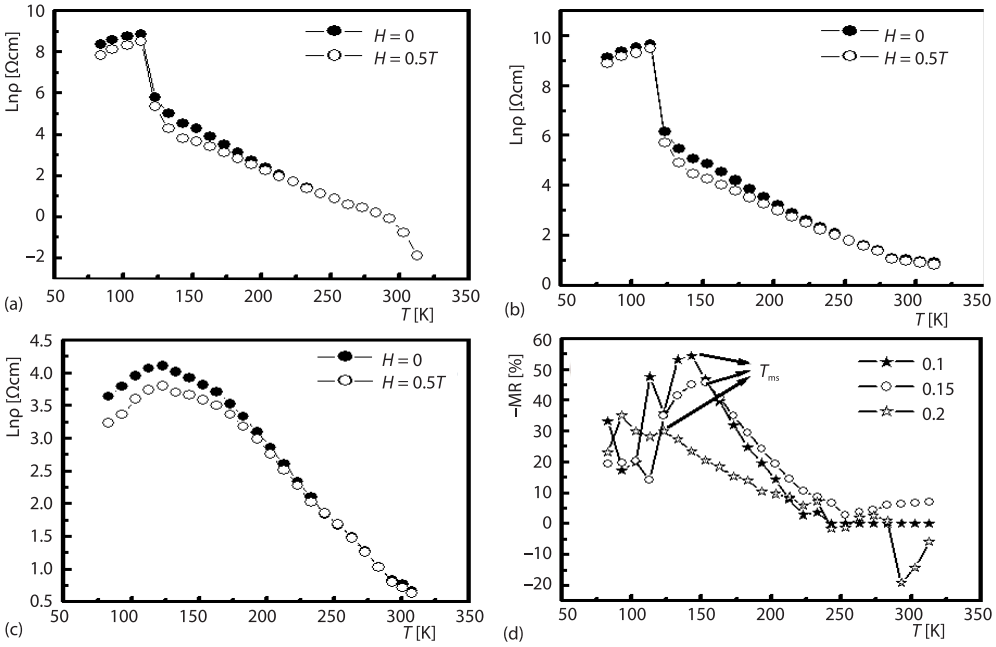

Figure 2. Temperature dependency of Ln(ρ) (at $H = 0$ and $0.5T$) for $La_{1-x}Sr_xMnO_3$; (a) $x = 0.1$, (b) $x = 0.15$, (c) $x = 0.2$, and (d) MR%

Noteworthy, for each composition, the lnρ-T plot measured at $H = 0.5T$ plot is always below that measured in zero field. This means resistivity declines by applying an external magnetic field because spins get favorably oriented, and charge carriers exhibit lower scattering throughout the process of hopping [21, 22]. This allowed us to calculate the negative MR using the relation:

$$\mathrm{MR} = \frac{\rho(H) - \rho(0)}{\rho(0)} \times 100 \tag{1}$$

where ρ(H) and $\rho(0)$ are the resistivity values with and without applying magnetic field, respectively.

Effect of annealing

Heat treatment is critical for perovskite materials where it can strongly influence their transport properties. Annealing process may change the defect concentration and thereby alter the carrier concentration besides its influence on the GS and grain orientation of samples under study therefore, one can understand that there is a tremendous influence of annealing on CS and electrical properties too.

The data gathered from fig. 2(d) suggests that the sample $x = 0.15$ has the greatest value of MR%. Therefore, the central issue addressed here is how we enhance this value at room temperature. The answer to this question makes our curiosity to investigate the impacts of thermal treatment on this particular sample. Figure 3 shows the relation between MR% and

temperature at different time intervals taking in our consideration the annealing temperature is 800 °C. Clearly, MR% increases with increasing annealing processes. This is evidence that this procedure has a positive influence on improving MR% especially at room temperature. This is a novel solution that develops the claim that the annealing process enhances the value of magnetoresistance especially, at room temperature.

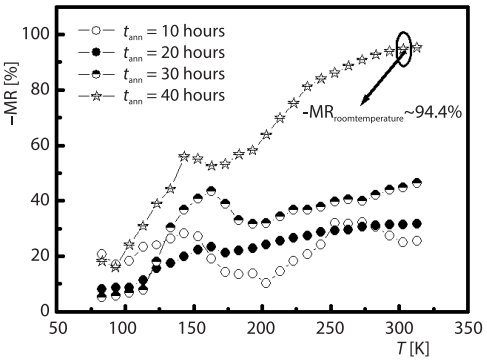

Figure 3. Temperature-dependent MR% of $La_{1-x}Sr_xMnO_3$ $x = 0.15$ annealed at 800 °C for 10 hours

For our samples, the paramagnetic/semiconducting region observed at $T > T_{ms}$ were categorized to two different conduction mechanisms. First category is at the range $T_{ms} \leq T \leq \theta D/2$, where θD is the Debye temperature. It is well-described by the VRH model whereas the second fits well with the small polaron hopping model and lies at $T > \theta D/2$ [23, 24]. The small polaronic model is given:

$$\frac{\rho}{T} = \rho_\alpha \exp \frac{E_\rho}{k_B T} \tag{2}$$

where E_ρ is the activation energy, k_B – the Boltzmann constant, and T – the absolute temperature. As known, E_ρ is given by [25]:

$$E_\rho = W_H + \frac{W_D}{2}\left(\text{for } T > \frac{D}{2}\right), \quad E_\rho = W_D\left(\text{for } T > \frac{D}{4}\right) \tag{3}$$

where W_H is the polaron hopping energy, W_D is the disorder energy. The parameters are calculated and presented in tab. 2. Obviously, for all compositions as x increases, θD and υ_{ph} increase while E_ρ and W_H decrease this because the increase of Sr content causes larger bandwidth which makes the charges to be in a delocalized state [26, 27]. Thus, the energy needed to liberate free carriers is reduced consequently [26]. Holstein's condition is employed determine whether the hopping is in the adiabatic or non-adiabatic state [28], according to the conditions:

$$\begin{aligned} J > H \ \ &\text{(for adiabatic condition)} \\ J < H \ \ &\text{(for } \textit{non}\text{-adiabatic condition)} \end{aligned} \tag{4}$$

$$H(T) = \left(\frac{2k_B T W_H}{\pi}\right)^{1/4} \left(\frac{h\upsilon_{ph}}{\pi}\right)^{1/2} \tag{5}$$

$$J(T) = 0.67 h\upsilon_{ph} \left(\frac{T}{\theta_D}\right)^{1/4} \tag{6}$$

Values of $H(T)$ and $J(T)$, obtained at room temperature, are illustrated in tab. 2. Since small polaron formation must satisfy the condition $J > W_H/3$ [28], one can conclude that the conduction in $La_{1-x}Sr_xMnO$ ($x = 0.1$, 0.15, and 0.2) is due to the small polaron hopping mechanism in non-adiabatic regime. Debye temperature θD was obtained via plots of temperature linearity of $\ln(\rho/T)$ *vs.* $1/T$ above T_{ms}, as shown in fig. 4.

Table 2. The parameters calculated from resistivity for $x = 0.1$, 0.15, and 0.2 at $T_{ms} \leq T \leq \theta D/2$

Sample	0.1	0.15	0.2
θ_D [K]	366.05	369.65	388.57
V_{ph} [Hz]	$7.61 \cdot 10^{12}$	$7.69 \cdot 10^{12}$	$8.08 \cdot 10^{12}$
ρ_a [Ωcm]	$0.771 \cdot 10^{-6}$	$3.61 \cdot 10^{-5}$	$4.38 \cdot 10^{-5}$
E_p [meV]	154.24	141.61	133.06
ΔE_s [meV]	6.299	13.078	4.637
W_H [meV]	147.95	128.54	128.42
$W_H/3$ [meV]	49.31	42.84	38.47
W_D [meV]	12.58	26.15	9.72
α (e/K_B)	–11.32	–35.40	–10.16
T_o [K]	86215860	35574936	4611307
N(E_f) [meV^{-1}cm^{-3}]	$2.21 \cdot 10^{26}$	$5.36 \cdot 10^{26}$	$4.13 \cdot 10^{27}$
R_h (300 K) [A°]	239.24	98.72	12.80
E_h [meV]	149.77	120.04	72.02
γ_p	9.38	8.07	7.67
exp(γ_p)	11877.78	3203.62	2148.28
J (300 K) [meV]	20.10	20.25	21.02
φ (300 K) [meV]	704.25	683.26	700.37

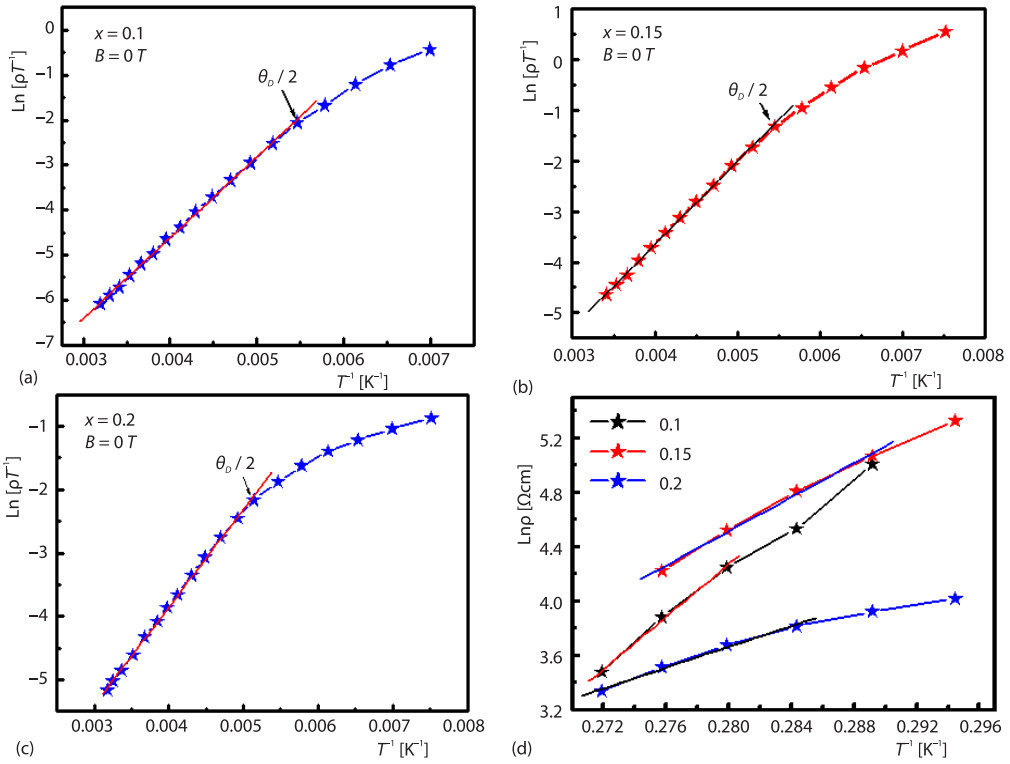

Figure 4. The SPH model of $La_{1-x}Sr_xMnO_3$; (a) $x = 0.1$, (b) $x = 0.15$, (c) $x = 0.2$, and (d) VRH model plot

Following the equation: $\gamma_p = 2W_H/h\upsilon_{\text{ph}}$ [29, 30], γ_p which helps in determination the electron-phonon-interaction can be estimated. As tabulated in tab. 2, the γ_p is higher than four implying a strong electron-phonon-interaction [26] but its contribution decreases with Sr content, see tab. 2. The relation between m_p and m^* is given by the equation [26].

$$m_p = \left(\frac{h^2}{8\pi JR^2}\right)\exp(\gamma_p) = m^* \exp(\gamma_p) \tag{7}$$

The values of m_p/m^* ratio presented in tab. 2 show that the mass of polaron decreases with elevation the Sr amounts. As shown in fig. 4 the Lnρ *vs*. $T^{-1/4}$ plots (for the data of temperature range $T_{\text{ms}} \leq T \leq \theta D/2$ are in linear form confirming well agreement of the conduction mechanism to the VRH model [31]. According to VRH model resistivity is written as [30, 32]:

$$\rho(T) = \rho_o \exp\left(\frac{T_o}{T}\right)^{1/4} \tag{8}$$

T_o is constant given by:

$$T_o = \frac{18}{k_B N(E_f) a^3} \tag{9}$$

where $N(E_f)$ is the determines density of states and a – the localization length with a value equal to 2.22 nm^{-1} [32]. Consequently, hopping distance $R_h(T)$ and hopping energy $E_h(T)$ are written as [33, 34]:

$$R_h(T) = \frac{3}{8} a \left(\frac{T_o}{T}\right)^{1/4} \tag{10}$$

$$E_h(T) = \frac{1}{4} k_B T^{3/4} T_o^{1/4} \tag{11}$$

Calculating the value of T_o allows us to estimate the value of $N(E_f)$, $R_h(T)$, and $E_h(T)$ at room temperature, see tab. 2. Obviously, increasing the Sr concentration makes the density of states to increase [26] and Mott characteristic temperature to decrease [27]. Furthermore, the hopping distance and hopping energy decrease with increasing strontium concentration. This may be caused to the lattice distortion due to the difference in ionic radii between La^{3+} ions (r = 117.2 pm) and Sr^{2+} (r = 132 pm) ions, which would lead to potential disorder [35].

Metallic behavior at low temperatures can be explained in terms of various scatterings [36].

The empirical equations were used to understand the conduction mechanisms at low temperatures [36-39]:

$$\rho = \rho_0 + \rho_2 T^2 + \rho_{4.5} T^{4.5} \tag{12a}$$

$$\rho = \rho_0 + \rho_2 T^2 + \rho_{4.5} T^{4.5} + \rho_5 T^5 \tag{12b}$$

where ρ_0 is the resistivity due to grain boundary effects and other defect features like dislocations, point defects, *etc*. [40], ρ_2 – the resistivity due to the electron-electron scattering process, and $\rho_{4.5}$ – the resistivity due to the electron-magnon-scattering. Finally, ρ_5 represents the resistivity due to electron-phonon-dispersion. The data of 0.1 and 0.15 compositions show best fitting to eq. (12a) this of the x = 0.2 composition are well represented by eq. (12b). The calculated parameters are tabulated in tab. 3. The parameter ρ_0 decreases sharply with increasing the Sr contents indicating a decrease in the grain boundary. The huge ρ_0 value of x = 0.15 composition (which is the largest ever) is attributed to the smallest GS, see tab. 3.

Table 3. The parameters calculated from data of the resistivity measurements for $x = 0.1$, 0.15, and 0.2 at $T < T_{ms}$

x	$\rho = \rho_0 + \rho_2 T^2 + \rho_{4.5} T^{4.5}$			$\rho = \rho_0 + \rho_2 T^2 + \rho_{4.5} T^{4.5} + \rho_5 T^5$			
	ρ_0	ρ_2	$\rho_{4.5}$	ρ_0	ρ_2	$\rho_{4.5}$	ρ_5
0.1	1959.82	1.062	2.749	–	–	–	–
0.15	5342.20	2.466	6.289	–	–	–	–
0.2	–	–	–	125.67	2.86	8.07	5.96

On the other side, the electron-electron scattering parameter ρ_2 increases with Sr doping level but with a smaller variation in comparison that of ρ_0. Generally, it appears from the $\rho_{4.5}$ and ρ_5 values that the electron-magnon-and electron-phonon-scattering contributions are comparable.

Thermoelectric power

Degenerate and non-degenerate state

The current debate revolves around the location of transition temperature whether in degenerate or non-degenerate state. Thermoelectric power (TEP) is the best technique to portray this issue. Clearly, from fig. 5 the see beck coefficient for all samples raises with the temperature increasing indicating a degenerate semiconductors behavior. A degenerate semiconductor behavior can be expressed as [41]:

$$S = \frac{\pi^2 k_B^2 T}{3eE_f} \tag{13}$$

This occurs at definite temperature T_s~175 K for all concentrations. On the other side, after this temperature Seebeck coefficient shows an expression [42]:

$$S_d = \frac{k_B}{e}\left[\frac{E_f}{k_B T} + \left(r + \frac{5}{2}\right)\right] \tag{14}$$

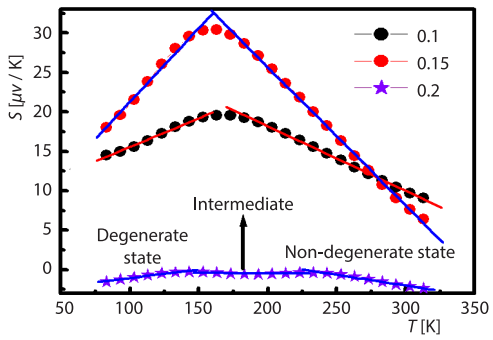

Figure 5. Temperature dependency TEP for $La_{1-x}Sr_xMnO_3$ $x = 0.1$, 0.15, and 0.2

On basis of the previous discussion, it seems that the transition temperature T_c or T_{ms} lay in the degenerate state. It is worth to be mentioned that fig. 5 give us an indication that both 0.1 and 0.15 samples transfer directly from degenerate and non-degenerate state after 175 K but for $x = 0.2$ there is intermediate state in range temperature 145 K < T < 245 K before the sample change to non-degenerate state.

To identify the contributing mechanism in the thermoelectric properties of the concerned compositions we recall fig. 6. Obviously, S-T curve can be represented by two parts the first one in low temperature ($T < T_s$) and the second part in high temperature ($T > T_s$) we will study each part in detail in the following sections.

High temperature region ($T > T_s$)

The semiconductor part (over the high temperature region), the S-T plots were found to be well represented with the expression:

$$S = \left(\frac{k_B}{e}\right)\left(\frac{\Delta E_s}{K_B T} + \alpha\right) \tag{15}$$

where ΔE_s is the activation energy, α – the constant, and e is the electron charge [43]. Over the whole paramagnetic-semiconducting the linearity confirms well-fitting of data to eq. (15). Note that, the *S vs*. $1/T$ plots (the plots are not shown here) correspond to only the highest temperature range and were used for calculating the thermopower activation energy ΔE_s, see tab. 2. It was presented previously that the highest temperature range ($T > \theta D/2$) is characterized with the small polaron hoping mechanism and the electrical conductivity activation energy E_p was calculated from the $\ln(\rho/T) - 1/T$ curves at this range, tab. 2. The difference between the values of E_p and ΔE_s is the polaron hopping energy W_H ($W_H = E_p - \Delta E_s$) [44]. The W_H values shown in tab. 2 demonstrate a fall down of the polaron hopping as the Sr content increases. On the other hand, being $\alpha < 1$ and $\Delta E_s < E_p$ this support the small polaron hopping conduction at the range $T > \theta D/2$ [45].

Low temperature region ($T < T_s$)

The coefficient of Seebeck in the ferromagnetic-metal FM region, analyzed by [46]:

$$S = S_o + S_{3/2}T^{3/2} + S_4 T^4 \tag{16}$$

where S_4T4 is dependent on the spin-wave fluctuations [47]. However, the aforementioned equation can be re-written [48]:

$$S = S_o + S_1 T + S_{3/2}T^{3/2} + S_3 T^3 + S_4 T^4 \tag{17}$$

Experimental results of all the compositions at hand were fitted to eq. (17) and the best-fit parameters obtained for all the samples are given in tab. 4. Clearly, no sequential change can be observed for any of the tabulated parameters. This means that over the whole temperature of measurements within the FM region, there is no thermopower mechanism contributes dominantly to our compositions.

Table 4. The thermopower parameters calculated from eqs. (5)-(17) over the whole temperature range of measurements

x	S_0	S_1	$S_{3/2}$	S_3	S_4
0.1	30.984	–0.704	5.645	9.567	–2.583
0.15	92.710	–3.815	0.355	–5.219	6.502
0.2	10.501	–0.708	7.134	–1.510	3.026

However, in the following we will prove that a certain mechanism can dominate over a certain temperature range. Figure 6(a) shows the phonon-drag components for all compositions. The phonon-drag component is dominant at the higher temperature range of the FM region. The deviation occurs in $x = 0.1$ and $x = 0.15$ in the lower temperature range due to the domination of the magnon-scattering on the expense of that of the phonon-drag. To confirm this conclusion, the magnon-scattering component dependence on $T^{3/2}$ is presented in fig. 6(b).

The data illustrates linear behavior in the lower temperature range. Decreasing the phonon-drag component with decreasing the temperature for $x = 0.1$ and $x = 0.15$ is reasonable may because the lattice approach to the frozen state at low temperature. Notably, $x = 0.2$ composition show unique linear behavior over the whole FM range whether for T^3 or $T^{3/2}$ dependency. This means that for these compositions the contribution of magnon-scattering and phonon-drags are comparable at the FM range.

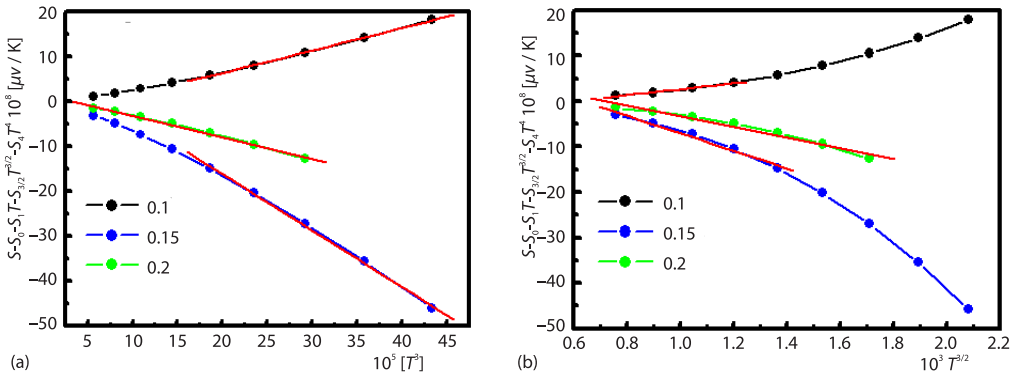

Figure 6. (a) Phonon-drag and (b) magnon-scattering dependence on T^3 and $T^{3/2}$, respectively of the compositions under study

Conclusion

Resistivity, magnetoresistance, thermoelectric power and magnetization properties were studied for $La_{1-x}Sr_xMnO_3$ (x = 0.1, x = 0.15, and x = 0.2) samples. Mechanism of conduction at ($T > T_{ms}$) of conductivity data was successfully fitted with the VRH in the range $\theta D/2 \geq T \geq T_{ms}$. The non-adiabatic SPH model was found to be applicable at $T > \theta D/2$. The data of Seebeck coefficient supports the transition between degenerate and non-degenerate regime below and above T_s, respectively. The contributing mechanisms below and above T_s has been studied in detail. The magnetization *vs.* temperature for LSMO system showed FM-PM transitions at a specific transition temperature, T_c. Magnetization *vs*. magnetic field measurement clarifies that all samples didn't show any hysteresis loop in the positive field cycle.

Acknowledgment

The work was supported by the Princess Nourah bint Abdulrahman University Researchers Supporting Project No. PNURSP2024R124, Princess Nourah bint Abdulrahman University, Riyadh, Saudi Arabia

References

[1] Dorr, K., Ferromagnetic Manganites: Spin-Polarized Conduction vs. Competing Interactions, *J. Phys. D, Appl. Phys*., *39* (2006), 125
[2] Ahmed, A. M., *et al*., The Annealing Influence on the Electrical and Magnetic Behavior of Magnetoresistive/Insulator System, *J. Low Temp. Phys*., *42* (2016), 9, pp. 951-958
[3] Jenker, G. H., van Santen, J. H., Ferromagnetic Compounds of Manganese with Perovskite Structure, *Physica*, *16* (1950), 337
[4] Jenker, G. H., van Santen, J. H., Electrical Conductivity of Ferromagnetic Compounds of Manganese with Perovskite Structure, *Physica*, *16* (1950), 599
[5] Zener, C., Interaction between the d-Shells in the Transition Metals, II Ferromagnetic Compounds of Manganese with Perovskite Structure, *Phys. Rev*., *82* (1951), 403
[6] Dinesh Varshney, D. N., Electrical Resistivity of the Hole Doped $La_{0.8}Sr_{0.2}MnO_3$ Manganites: Role of Electron-Electron/Phonon-/Magnon-Interactions, *Mate. Chem. Phys*., *129* (2011), 3, pp. 896-904
[7] Ahmed, A. M., *et al*., Enhanced Electro-Magnetic Properties in $La_{0.7}S_{r0.3}MnO_3/ZrO_2$ Composites, *Indian J. Phys*., *89* (2015), 6, pp. 561-570
[8] De Teresa, J. M. *et al*., Evidence for Magnetic Polarons in the Magnetoresistive Perovskites, *Nature*, *386* (1997), Mar., pp. 256-259
[9] Rao, C. N. R., Rachaudhuri, A. K., Colossal Magnetoresistance, *Charge Ordering and Other Novel Properties of Manganites and Related Materials*, *1* (1998), 13

[10] Mollah, S., *et al.*, Adiabatic Small Polaron-Hopping Conduction in $Ln_{0.85}Ca_{0.15}MnO_3$ (Ln=Nd, Pr and Sm) Perovskites, *J. Phys. Chem. Solids*, *69* (2008), 1023
[11] Iguchi, E., *et al*., Correlation between Hopping Conduction and Transferred Exchange Interaction in La_2NiO_4+δ below 300 K, *Physica B*, (1999), 3-4, pp. 270-332
[12] Tabuchi, A., *et al*., Dielectric Relaxation in $LaSrCo_{1-x}Al_xO_4$ Ceramics, *J. All. Compo*., *1214* (2006), May, pp. 408-412
[13] Adam, A. M., *et al*., Effects of Transition Metal Element Doping on the Structural and Thermoelectric Properties of n-Type $Bi_{2-x}Ag_xSe_3$ Alloys, *J. All. Compo*., *851* (2021), 156887
[14] Ahmed, A. M., *et al*., Crystal Structure and Some Transport Properties of Na-Doped $LaMnO_y$, *J. Magm. Magn. Mater*., *301* (2006), 452
[15] Mahesh, R., *et al*., Effect of Particle Size on the Giant Magnetoresistance of $La_{0.7}Ca_{0.3}MnO_3$, *Appl. Phys. Lett.*, *68* (1996), 2291
[16] Roy, S., *et al*., Interplay of Structure and Transport Properties of Sodium-Doped Lanthanum Manganite, *J. Phys. Condens. Matter.*, *13* (2001), 9547
[17] Kouta, I., *et al*., Thermoelectric Properties of Polycrystalline $La_{1-x}Sr_xCoO3$, *Solid State Chem*., *181* (2008), 11, pp. 3145-3150
[18] JDhahri, J., *et al*. The Effect of Deficit of Strontium on Structural, Magnetic and Electrical Properties of $La_{0.8}Sr_{0.2-x}$·$xMnO_3$ Manganites, *J. All. Compo*., *394* (2005), 1-2, pp. 51-57
[19] Zemni, S., *et al*., The Effect of a Cation Radii on Structural, Magnetic and Electrical Properties of Doped Manganites $La_{0.6-x}Pr_xSr_{0.4}MnO_3$, *J. Solid State Chemistry*, *177* (2004), 7, pp. 2387-2393
[20] Elsehly, E. M., *et al*., Annealing Effect on the Thermoelectric Properties of Multiwall Carbon Nanotubes, *Physica E: Low-Dimensional Systems and Nanostructures*, *146* (2023), 115566
[21] Dutta, A., Effect of Particle Size on the Magnetic and Transport Properties of $La_{0.875}Sr_{0.12}5MnO_3$, *Phys. Rev. B*, *68* (2003), 054432
[22] Furukawa, N., Transport Properties of the Kondo Lattice Model in the Limit S = ∞ and D = ∞, *J. Phys. Soc. Jpn*., *63* (1994), 3214
[23] Rao, C. N. R., Raychaudhur, A. K., *Colossal Magneto- Resistance*, *Charge Order and Other Novel Properties of Manganites and Related Materials*, World Scientific Publishing, Singapur, Singapur, 1998, p. 7
[24] Mannella, N., *et al.*, Direct Observation of High-Temperature Polaronic Behavior in Colossal Magnetoresistive Manganites, *Phys. Rev. Leters*, *92* (2004), 16
[25] Sun, C. H., *et al.*, The Transport Properties in $Nd_{0.75}Sr_{1.25}CoO_4$ Film Evidence for Polaronic Transport, *J. Phys. Chem. Solids*, *70* (2009), pp. 286-290
[26] Austin, I. G., Mott, N. F., Polarons in crystalline and Non-Crystalline Materials, *Adv. Phys*., *18* (1969), 41
[27] Mollah, S., *et al*., Non-Adiabatic Small-Polaron Hopping Conduction in $Pr_{0.65}Ca_{0.35-x}Sr_xMnO_3$ Perovskites above the Metal-Insulator Transition Temperature, *J. Magm. Magn. Mater*., *284* (2004), 1, pp. 383-394
[28] Soma, D., Dey, T. K., Thermoelectric Power of Potassium Doped Lanthanum Manganites at Low Temperatures, *J. Magm. Magn. Mater*., *311* (2007), 2, pp. 714-723
[29] Jaime, M., *et al*., High-Temperature Thermopower in $La_{2/3}Ca_{1/3}MnO_3$ Films: Evidence for Polaronic *Transport. Phys. Rev. B*, *54* (1996), 11914
[30] Banerjee, P. S., Polaron Hopping Conduction and Thermoelectric Power in $LaMnO_{3+\delta}$, *J. Appl. Phys*., *89* (2001), 4955
[31] Viret, M., *et al.*, Magnetic Localization in Mixed-Valence Manganites, *Phys. Rev. B*, *55* (1996), 8067
[32] Ravi, S., Kar, M., Study of Magneto-Resistivity in $La_{1-x}Ag_xMnO_3$, *Compounds. Physica B*, *348* (2004), 169
[33] Khan, W., *et al*., Small Polaron Hopping Conduction Mechanism in Fe Doped $LaMnO_3$, *J. Chem. Phys. 135* (2011), 054501
[34] Jung, W. H., Magnetic and Transport Properties of $Ce_{2/3}TiO_{2.981}$, *J. Condens. Matter Phys*., *17* (1998), 1317
[35] Banerjee, A., Nature of Small-Polaron Hopping Conduction and the effect of Cr Doping on the Transport Properties of Rare-Earth Manganite $La_{0.5}Pb_{0.5}Mn_{1-x}CrxO_3$,*J. Chem. Phys*., *115* (2001), 1550
[36] Ahmed, A. M., Influence of Heat Treatment on the Magnetic and Magnetocaloric Properties in $Nd_{0.6}Sr_{0.4}MnO_3$ Compound, *Solid State Sci*., *57* (2016), July, pp. 1-8
[37] Abd El-Moez, A., Magnetoresistive and Magnetocaloric Response of Manganite/Insulator System, *J. Alloys Compd*., *657* (2016), Feb., pp. 495-505
[38] Venkataiah, G., Venugopal Reddy, P., Electrical Behavior of Sol-Gel Prepared $Nd_{0.67}Sr_{0.33}MnO_3$ Manganite System, *J. Magn. Magn. Mater*., *285* (2005), 3, pp. 343-352

[39] Sagdeo, P. R., *et al*., The Contribution of Grain Boundary and Defects to the Resistivity in the Ferromagnetic State of Polycrystalline Manganites, *J. Magn. Magn. Mate*r., *306* (2006), 1, pp. 60-68
[40] Y. Kalyana Lakshmi, P. Venugopal Reddy, Electrical Behavior of Some Silver-Doped Lanthanum-Based CMR Materials, *J. Magn. Magn. Mater.*, *321* (2009), 9, pp. 1240-1245
[41] Adam, A. M., et al., Thermoelectric Power Properties of Ge doped PbTe Alloys, *J. Alloys Compd.*, *872* (2021), 159630
[42] Nolas, G. S., *et al*., *Thermoelectrics Basic Principles and New Materials Developments*, Springer Series in Materials Science, Heidelberg, Germany, 2001, Vol. 45
[43] Jaime, M., *et al.*, Magnetothermopower in $La_{0.67}Ca_{0.33}MnO_3$ Thin Films, *Appl. Phys. Lett*., *68* (1996), 1576
[44] Mollah S., Non-Adiabatic Small-Polaron Hopping Conduction in $Pr_{0.65}Ca_{0.35-x}Sr_xMnO_3$ Perovskites above the Metal-Insulator Transition Temperature, *J. Magn. Magn. Mater*., *284* (2004), 1, pp. 383-394
[45] Ravi, S., Kar, M., Study of Magneto-Resistivity in $La_{1-x}Ag_xMnO_3$ Compounds, *Physica B*, *348* (2004), 169
[46] Mandal, P., Emperature and Doping Dependence of the Thermopower in $LaMnO_3$, *Phys. Rev.* B, *61* (2000), 14675
[47] Bhattacharya, S., *et al.*, Effect of Li Doping on the Magnetotransport Properties, of $La0.7Ca_{0.3-y}Li_yMnO_3$ System: Decrease of Metal-Insulator Transition Temperature, *Appl. Phys. Lett*., *82* (2003), 4103
[48] Kim, H. B., *et al*., Magnon-Drag Effect as the Dominant Contribution the Thermopower in $Bi_{0.5-x}La_{x}Sr_{0.5}MnO_3$ ($0.1 \leq x \leq 0.4$), *J. Appl. Phys*., *103* (2008), 3717

Paper submitted: August 24, 2024
Paper revised: October 27, 2024
Paper accepted: November 19, 2024